

Article

Temperature-Dependent Activity of Gold Nanocatalysts Supported on Activated Carbon in Redox Catalytic Reactions: 5-Hydroxymethylfurfural Oxidation and 4-Nitrophenol Reduction Comparison

Stefano Scurti ^{1,2}, Alessandro Allegri ^{1,2}, Francesca Liuzzi ^{1,2}, Elena Rodríguez-Aguado ³, Juan Antonio Cecilia ³, Stefania Albonetti ^{1,2,*}, Daniele Caretti ^{1,2,*} and Nikolaos Dimitratos ^{1,2,*}

¹ Industrial Chemistry “Toso Montanari” Department, University of Bologna, Viale Risorgimento 4, 40136 Bologna, Italy; stefano.scurti2@unibo.it (S.S.); alessandro.allegri2@unibo.it (A.A.); francesca.liuzzi7@unibo.it (F.L.)

² Center for Chemical Catalysis-C3, Alma Mater Studiorum Università di Bologna, Viale Risorgimento 4, 40136 Bologna, Italy

³ Departamento de Química Inorgánica, Cristalografía y Mineralogía (Unidad Asociada al ICP-CSIC), Facultad de Ciencias, Campus de Teatinos, Universidad de Málaga, 29071 Málaga, Spain; aguadoelena5@gmail.com (E.R.-A.); jacecilia@uma.es (J.A.C.)

* Correspondence: stefania.albonetti@unibo.it (S.A.); daniele.caretti@unibo.it (D.C.); nikolaos.dimitratos@unibo.it (N.D.)



Citation: Scurti, S.; Allegri, A.; Liuzzi, F.; Rodríguez-Aguado, E.; Cecilia, J.A.; Albonetti, S.; Caretti, D.; Dimitratos, N.

Temperature-Dependent Activity of Gold Nanocatalysts Supported on Activated Carbon in Redox Catalytic Reactions: 5-Hydroxymethylfurfural Oxidation and 4-Nitrophenol Reduction Comparison. *Catalysts* **2022**, *12*, 323. <https://doi.org/10.3390/catal12030323>

Academic Editor: Francesco Mauriello

Received: 8 February 2022

Accepted: 8 March 2022

Published: 11 March 2022

Publisher's Note: MDPI stays neutral with regard to jurisdictional claims in published maps and institutional affiliations.



Copyright: © 2022 by the authors. Licensee MDPI, Basel, Switzerland. This article is an open access article distributed under the terms and conditions of the Creative Commons Attribution (CC BY) license (<https://creativecommons.org/licenses/by/4.0/>).

Abstract: In this study, the temperature-dependent activity of Au/AC nanocatalysts in redox catalytic reactions was investigated. To this end, a series of colloidal gold catalysts supported on activated carbon and titania were prepared by the sol immobilization method employing polyvinyl alcohol as a polymeric stabilizer at different hydrolysis degrees. The as-synthesized materials were widely characterized by spectroscopic analysis (XPS, XRD, and ATR-IR) as well as TEM microscopy and DLS/ELS measurements. Furthermore, 5-hydroxymethylfurfural (HMF) oxidation and 4-nitrophenol (4-NP) reduction were chosen to investigate the catalytic activity as a model reaction for biomass valorization and wastewater remediation. In particular, by fitting the hydrolysis degree with the kinetic data, volcano plots were obtained for both reactions, in which the maximum of the curves was represented relative to hydrolysis intermediate values. However, a comparison of the catalytic performance of the sample Au/AC_PVA-99 (hydrolysis degree of the polymer is 99%) in the two reactions showed a different catalytic behavior, probably due to the detachment of polymer derived from the different reaction temperature chosen between the two reactions. For this reason, several tests were carried out to investigate deeper the observed catalytic trend, focusing on studying the effect of the reaction temperature as well as the effect of support (metal–support interaction) by immobilizing Au colloidal nanoparticles on commercial titania. The kinetic data, combined with the characterization carried out on the catalysts, confirmed that changing the reaction conditions, the PVA behavior on the surface of the catalysts, and, therefore, the reaction outcome, is modified.

Keywords: gold colloidal nanoparticles; hydrogenation of 4-nitrophenol; HMF oxidation; PVA hydrolysis degree

1. Introduction

In recent years, inorganic nanostructured materials have emerged as suitable heterogeneous catalysts for the industrial-scale production of value-added chemicals [1–5]. However, a specific design for high-performing nanocatalysts resulted in more complex structures due to a large number of variables such as catalytic environment and the dynamic mass- and energy-transport processes at the solid–liquid or solid–gas interfaces [6–8]. A more organic approach that includes the multifaceted role of the support along with

the tunability of nanoparticles (NPs) themselves offers new strategies for the design and performance optimization of heterogeneous nanocatalyst systems [9–11]. Thus far, a series of methodologies to synthesize NPs and nanoalloys with full control of their shapes and sizes has resulted in widespread applications in engineering, medicine, and catalysis [12–16]. The effect of particle size, topology, and surface crystal facets on the catalytic activity of noble metal nanocatalysts has been well documented and reviewed [17–22]. However, wet-chemical preparation involves the utilization of specific ligands that can bind the surface of nanocatalysts to tune the nanostructures and prevent the aggregation phenomena by lowering the free energy of the metal surface [23–25]. In fact, when NPs start agglomerating, they tend to become bulk-like materials and lose their peculiar features; therefore, a number of fundamental research have been carried out based on stabilization strategies [23,26]. Polymeric coating of colloidal particles is a robust and effective technique for imparting colloidal stability. The use of polymeric stabilizers such as polyvinyl alcohol (PVA), polyvinyl pyrrolidone (PVP), and polyethylene oxide (PEG) was widely investigated in different catalytic materials and reactions [27,28]. In particular, PVA exhibits properties such as hydrosolubility, biodegradability, and biocompatibility, which are more interesting to design a catalytic material by its synthesis in water media [29–31]. The conformation of surface ligands on a confined NP surface is largely determined by the chain length/charge/density of ligands and nanoparticles' surfaces. In addition, novel studies have focused on the effective role of the polymers in the catalytic mechanism in terms of active phase coverage, selectivity tuning, and promotion effect mediated by defined functional groups [17]. Chen et al. prepared coated ultrathin platinum nanowires and investigated the presence of interfacial electronic effects derived from organic capping during catalytic hydrogenation [32]. Furthermore, Zhang et al. described the role of ligands on the d-charge distribution in gold nanoparticles [33]. Shafer et al. showed the possibility to perform enantioselective hydrogenation modifying the structure of polymers used in supported Pd catalysts [34]. In this topic, polymeric stabilizers used in the synthesis of nanostructured materials can play significant roles in controlling catalytic activity and catalyst stability and could be offered as a “toolbox” for designing highly effective and stable catalysts. Recently, several researchers have focused on supported catalysts based on noble metals (Pd, Pt, Ru, or Au) or their combination (bimetallic systems) for the conversion of biomass and derivatives due to their role as potential alternatives to the traditional fossil sources to produce fuels and chemicals [35–39]. The oxidation of lignocellulosic platform molecules to value-added chemicals has been laid out as an efficient pathway for the valorization of biomass-based compounds. Among them, 5-hydroxymethylfurfural (HMF), produced by fructose or glucose dehydration, is considered to be a versatile chemical bio-based platform compound and, therefore, is a key precursor for the synthesis of important biomass-based furanic compounds with widespread applications. The oxidation of HMF to 2,5-furandicarboxylic acid (FDCA) is an impressive strategy to obtain a bio-based monomer for the polymer industry [40]. For instance, polyethylene 2,5-furandicarboxylate (PEF) is an excellent biopolymer alternative to polyethylene terephthalate (PET), which is obtained from fossil-based monomer terephthalic acid. In our previous study, we synthesized active carbon-supported Au species by using poly(vinyl alcohol-co-vinyl acetate) stabilizer prepared by the sol immobilization technique [41]. Unprecedented catalytic activity and stability were obtained with these catalytic materials in the reduction of 4-nitrophenol to 4-aminophenol. This reaction proceeds under mild conditions, and it is used as a model because is well controlled in the presence of the NPs without forming by-products and side-products and that the kinetics analysis is easily monitored by UV–Vis spectroscopy. A volcano plot was observed linking the catalytic performance with the hydrolysis degree of the polymeric stabilizers, and the maximum of the curve was identified at intermediate values. By these findings, we emphasize the importance of ligand–nanoparticle interrelationships in the catalytic mechanism of supported nanoparticles. Based on these premises, the aim of this paper was centered on a critical comparison between the catalytic activity observed for HMF oxidation and 4-nitrophenol reduction mediated by gold nanoparticles

supported on activated carbon. The effect of customized poly(vinyl alcohol-co-vinyl acetate) stabilizers on the catalytic activity in terms of conversion, selectivity, and availability of active sites on the metal surface of supported gold nanocatalysts is also discussed. In addition, a temperature-dependent study was conducted in order to investigate the stability of nanostructured materials and the effect of support using commercial titania and its effect on the catalytic performance in the chosen redox reactions.

2. Results

2.1. Characterization of Catalysts

A series of Au/AC catalysts were prepared and extensively characterized in a previous study via sol immobilization using PVA as a stabilizing agent and focusing on studying the effect of hydrolysis degree in terms of formation of Au nanoparticles and catalytic performance for the catalytic reduction of nitrophenol [41]. The PVA used had different hydrolysis degrees, varying from 20% to 99%. By the characterization techniques employed and evaluation of catalytic performance, a correlation between the hydrolysis of the polymeric coating and the average Au nanoparticle size was observed. In particular, from the TEM analysis, it was evident that the presence even of a minor quantity of hydroxyl groups in PVA could lead to an increase in the average Au particle size. The same trend was identified following the redshift of localized plasmon peaks of the Au colloidal nanoparticles. Additionally, a peculiar volcano plot was obtained through the fitting of the hydrolysis degree with the percentage of surface Au coverage in which the maximum of the curve corresponded to the sample prepared using a PVA with a hydrolysis degree of 60%. The prepared catalysts, along with their main characteristics, are listed in Table 1.

Table 1. TEM and XPS analysis of the synthesized fresh catalysts along with their main characteristics. PVA: origin of the polymer used as stabilizing agent, either commercial or synthesized ad hoc; PVA HD: hydrolysis degree of the polymer used; TEM $\bar{\phi}$: mean Au particle size, measured via TEM; Surface Au: gold percentage of surface atoms, measured via XPS.

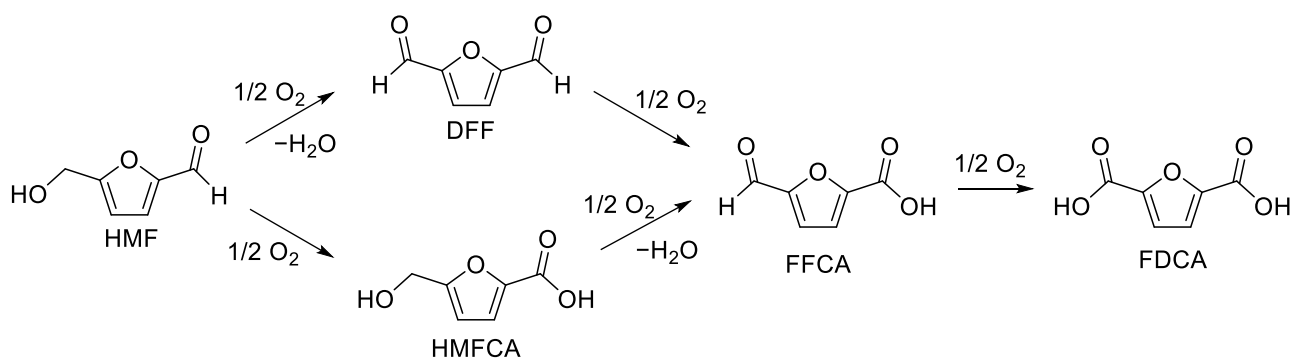
Sample	PVA	PVA HD (%)	TEM $\bar{\phi}$ (nm)	Surface Au (at%)
Au/AC_PVA-20	Synthesized	20	9.6	0.86
Au/AC_PVA-40	Synthesized	40	4.3	1.33
Au/AC_PVA-50	Synthesized	50	4.2	1.72
Au/AC_PVA-60	Synthesized	60	3.9	3.34
Au/AC_PVA-88	Commercial	88	3.4	2.04
Au/AC_PVA-99	Commercial	99	3.2	1.47

2.2. Catalytic Tests on HMF Oxidation

Each of the synthesized catalysts was tested in the selective oxidation of 5-hydroxymethylfurfural (HMF). Before testing the catalysts, blank tests were conducted, and both in absence of a catalyst and in presence of only activated carbon, the only reaction that occurred was the degradation of HMF in agreement with our previous research [37]. In comparison, the presence of a catalyst promoted the oxidation of HMF to 5-hydroxymethylfuran carboxylic acid (HMFCa), the first intermediate depicted in Scheme 1, a parallel product of 2,5-diformylfuran (DFF), which was not observed due to the basic conditions in which the reaction is conducted. The subsequent oxidation of HMFCa led to 5-formylfuran carboxylic acid (FFCA) and finally to 2,5-furandicarboxylic acid (FDCA), the final product of the reaction. FFCA was only detected in very small quantities since its formation from HMFCa is the rate-determining step of the process, and further oxidation of FFCA to FDCA is fast [37,42].

The results in Figure 1 and Table S1 show that HMF conversion was complete for each PVA hydrolysis degree, and FFCA selectivity was always negligible. This confirmed that HMFCa oxidation was the slowest step of the process. For these reasons, FDCA

selectivity can be considered representative of the catalytic activity when comparing the different catalysts.



Scheme 1. Reaction pathway for the selective oxidation of HMF.

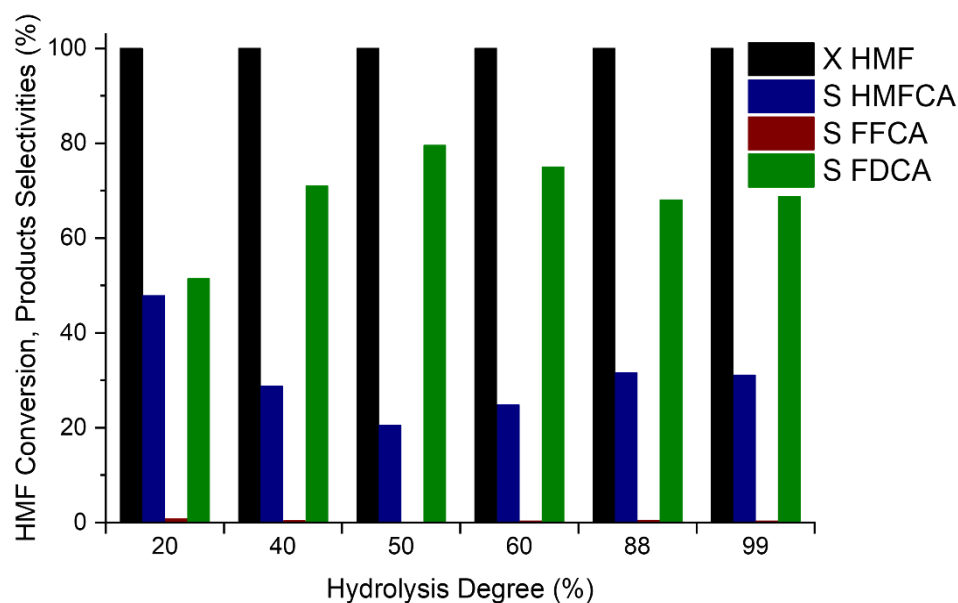


Figure 1. Effect of hydrolysis degree on the catalytic performances for HMF oxidation. Reaction conditions: $T = 70 \text{ }^\circ\text{C}$, $t = 4 \text{ h}$, $P = 10 \text{ bar O}_2$, molar ratios HMF: Au: NaOH = 1:0.01:4.

The FDCA selectivity increased with the hydrolysis degree up to 50%, after which it decreased again. Comparing this selectivity trend with mean Au particle size, as measured by TEM analysis (Figure 2), it is possible to detect a degree of correlation for lower hydrolysis degrees (up to 50%); smaller nanoparticles were more active. At higher hydrolysis degrees, this correlation was not evident, suggesting the prevalence of a different effect. The main contribution of the additional effect could be related to the solubility of the polymer, which could influence the catalytic activity as a function of reaction time.

Since PVA-88 and PVA-99 are commercial polymers, while the PVA samples with HD = 20–60% were synthesized, it is possible to observe that a lower hydrolysis degree in the stabilizing polymer (i.e., in the 50–60% range) led to catalysts with higher selectivity to FDCA (80% and 75% for HD = 50% and HD = 60%, respectively) than those prepared with commercial polymers (68% and 69% for HD = 88% and HD = 99%, respectively). In order to assess the stability of the catalysts, both the best-performing catalyst (Au/AC_PVA-50) and a reference one prepared with a commercial polymer (Au/AC_PVA-88) were employed in a reusability test. The catalysts were employed in three subsequent reaction cycles. In order to better assess any possible change in the catalyst's behavior, the reaction time was decreased to 2 h for these reactions so that the FDCA selectivity achieved by Au/AC_PVA-50 on the first use was closer to 50%. The results reported in Figure 3 show a decrease in

selectivity to FDCA with each cycle, consistent with the results reported in the literature, but no significant difference was observed in the behavior of the two catalysts [42].

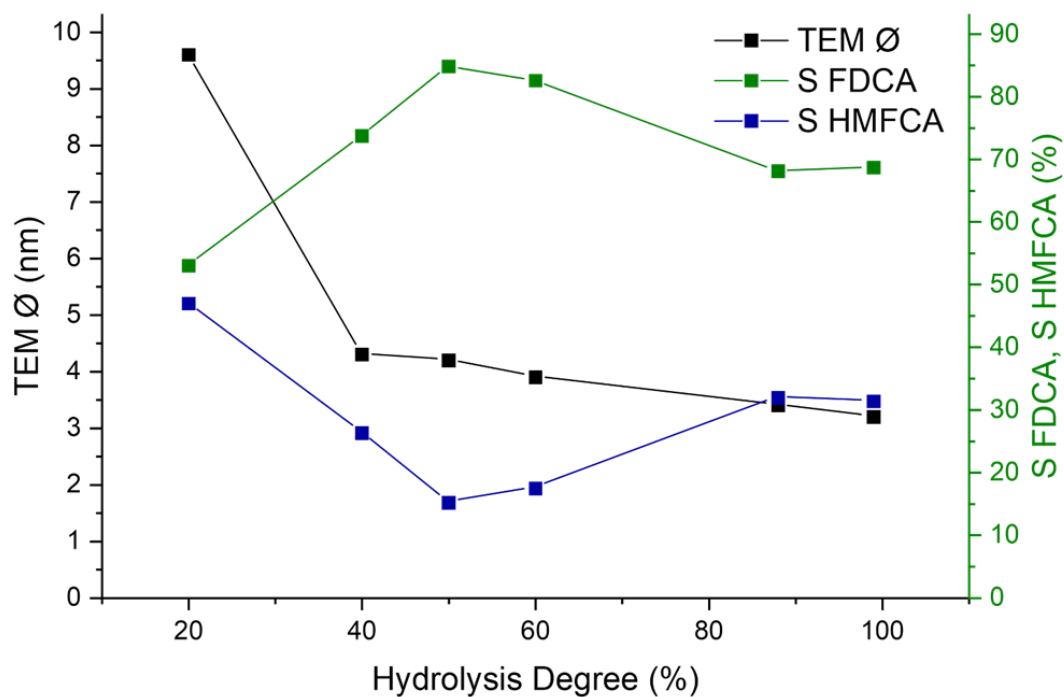


Figure 2. Correlation between mean particle diameter (TEM Ø, in black) and FDCA selectivity (S FDCA, in green) while changing the hydrolysis degree.

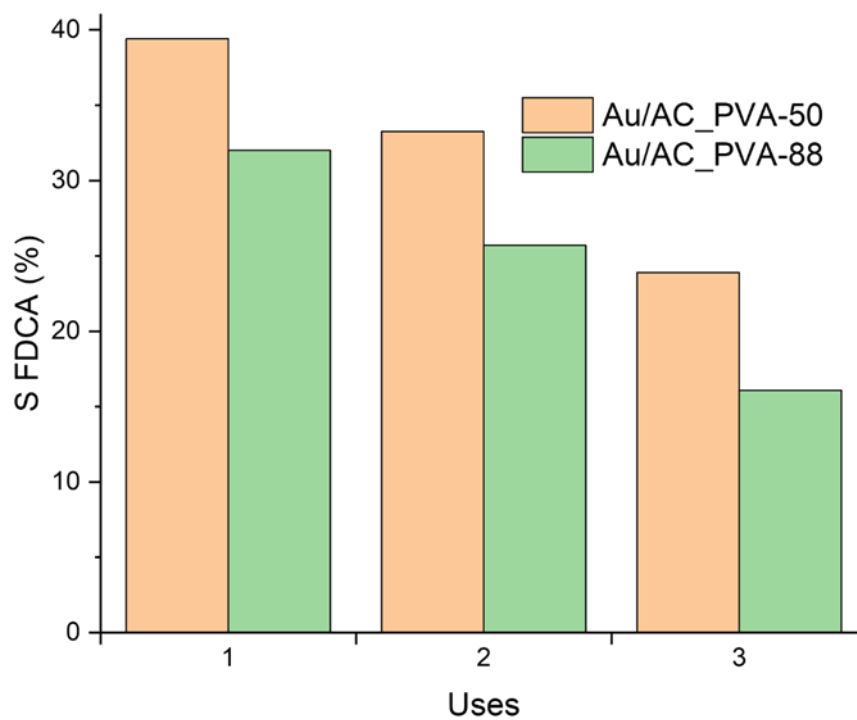
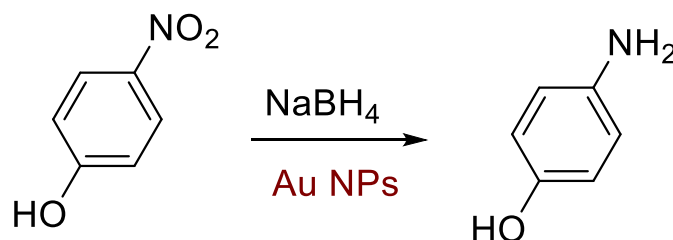


Figure 3. Reusability tests on HMF oxidation using two catalysts prepared with either a synthesized or a commercial polymer. Reaction conditions: $T = 70\text{ }^{\circ}\text{C}$, $t = 2\text{ h}$, $P = 10\text{ bar O}_2$, molar ratios HMF: Au: NaOH = 1:0.01:4.

2.3. Catalytic Tests on 4-Nitrophenol Reduction

The catalysts used for the HMF oxidation were tested previously in the 4-nitrophenol (4-NP) reduction to 4-aminophenol (4-AP), with an excess of sodium borohydride (Scheme 2). Indeed, in the presence of sodium borohydride, 4-NP was promptly deprotonated, to quantitatively yield the 4-nitrophenolate anion, which had a very characteristic absorption spectrum, with a maximum of 400 nm. The 4-NP anion could then be reduced to 4-AP in the presence of an appropriate catalyst. This reduction could easily be studied by means of UV-Vis spectroscopy by continuously measuring the absorbance of the solution at 400 nm [43–45].



Scheme 2. Reaction scheme for the 4-Nitrophenol (4-NP) reduction to 4-Aminophenol (4-AP).

Conducting the reaction in presence of a large excess of reducing agent, it is possible to consider its concentration as constant so that the kinetic equation describing the process can be expressed as pseudo-first-order [13,46,47]. It is then possible to fit the kinetic curves to calculate the kinetic constants. This was carried out for each of the prepared catalysts, and the results are reported in Figure 4 and Table S2.

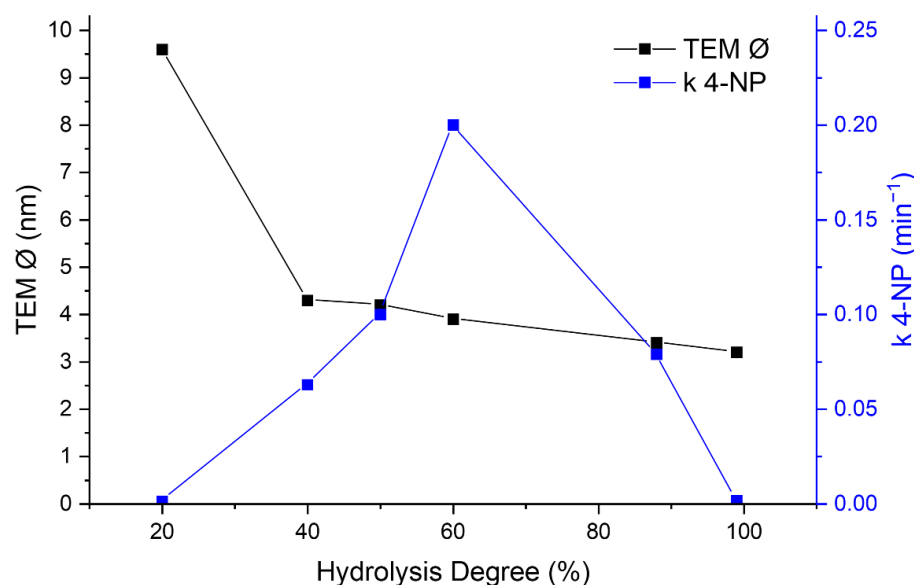


Figure 4. Effect of the PVA hydrolysis degree on the mean particle diameter (TEM Ø, in black) and the 4-NP reduction pseudo-first-order kinetic constant (k 4-NP, in blue).

Based on a comparison of the pseudo-first-order kinetic constants, it is clear that the main factor influencing the activity of the catalysts regarding the reduction of 4-NP was not simply the particle size. A significant decrease in mean Au particle size when the hydrolysis degree varied from 20% to 40% was followed by an increase in apparent kinetic constant. Moreover, a further increase in the apparent kinetic constant was observed from 40% to 50%, despite the mean Au particle size not decreasing significantly. Comparing the catalytic performances of the series of catalysts in the two different reactions (Figure 5), a similar trend was observed: Intermediate hydrolysis degrees yielded better catalytic

performance for both reactions. Despite the similarity in the two trends, there were two main differences. Firstly, a clear shift could be seen—namely, the optimal PVA hydrolysis degree for HMF oxidation was around 50%, while PVA with a 60% hydrolysis degree led to the highest catalytic performance in 4-NP reduction. The second difference was that the catalysts with the highest and lowest hydrolysis degrees of PVA showed almost no activity in 4-NP reduction, while the performances in HMF oxidation were remarkable even in the worst cases.

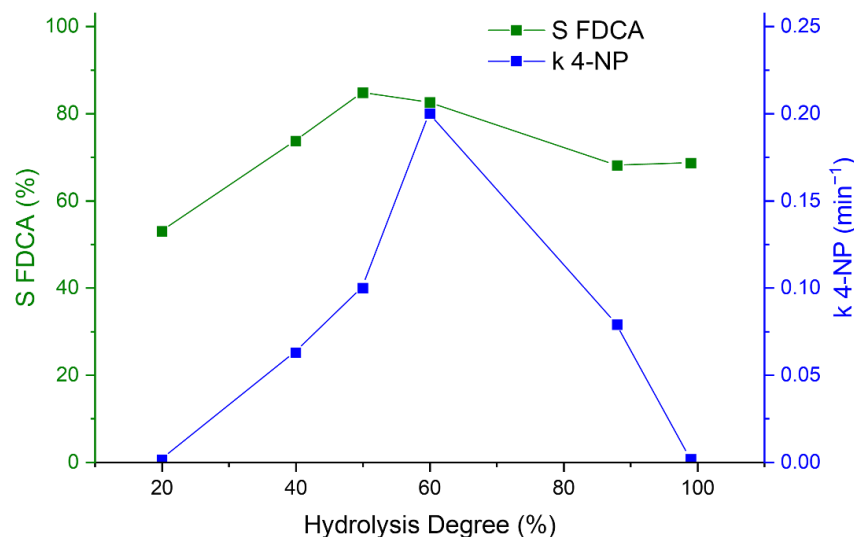


Figure 5. Correlation between FDCA selectivity (S FDCA, in green) and 4-NP reduction pseudo-first-order kinetic constant (k 4-NP, in blue) with changing hydrolysis degree.

In order to explain these differences, the effect of the stabilizing agent on the surface of the nanoparticles should be considered. In order to quantify the prevalence of this effect, XPS analysis was conducted for the series of Au catalysts. In Figure 6, the surface abundance of Au resulting from XPS measurements is plotted. Alongside surface Au, the catalytic performances in the two reactions are plotted as well.

From Figure 6, it is evident that there was a correlation between surface Au and 4-NP reduction kinetic constant. This suggests that, for the catalytic reduction of 4-NP, the limiting factor might not be the intrinsic activity of the gold nanoparticles, but instead, it could be the diffusion rate through the polymeric shell around the active phase. This effect was not present in HMF oxidation, and the catalytic performance of the Au catalysts was much more closely correlated to the values of mean gold particle size and, to a lesser extent, to the Au surface coverage.

The difference between these two catalytic behaviors seems to be due to the two opposing effects of PVA as a capping agent: The first is its obvious and desired function in preventing particle growth during the synthesis of Au NPs, while the second is its detrimental effect as a barrier hindering reagents diffusion to the gold nanoparticles. This effect seemed to be much more prevalent in the case of 4-NP reduction rather than in the HMF oxidation. This was hypothesized to be due to the different reaction temperatures that the two reactions were conducted; the 4-NP catalytic reduction was carried out at room temperature, whereas in the case of HMF oxidation, a higher reaction temperature (70 °C) was required. At higher reaction temperature, PVA could be solubilized to a higher degree, and therefore, its detachment from the surface of the Au NPs was promoted. During the reaction at the higher reaction temperature, the surface Au coverage was varied, and therefore, the higher accessibility of Au active sites could be the reason for observing catalytic activity for HMF oxidation at low and high hydrolysis degrees. Moreover, for both reactions, a similar trend was observed in terms of mean Au particle size and Au surface coverage. A decrease in mean Au particle size and increase in surface Au coverage was accompanied by an increase in catalytic activity.

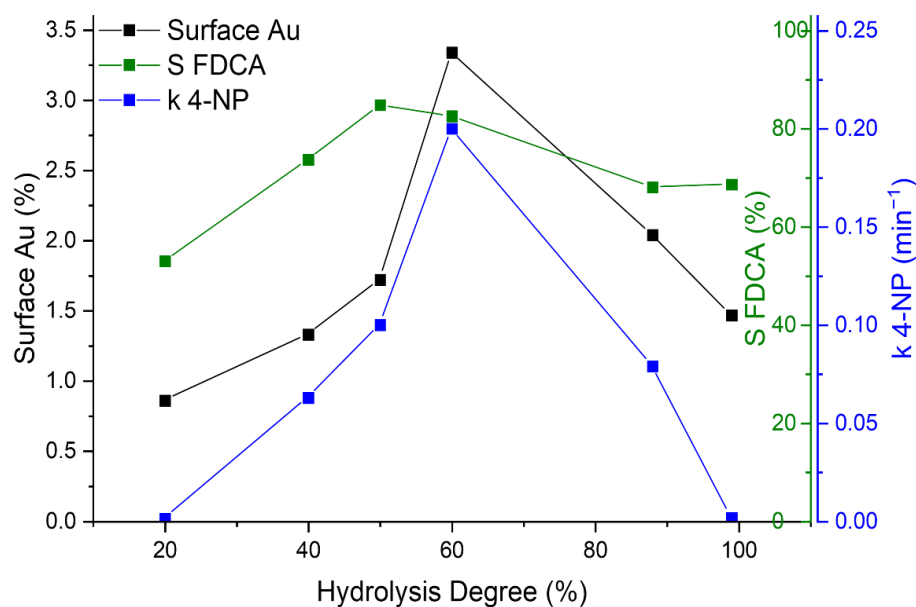


Figure 6. Comparison of the effects of hydrolysis degree on surface exposition of gold from XPS (in black), selectivity toward FDCA (in green), and 4-NP reduction pseudo-first-order kinetic constant (in blue).

To investigate the stability of the prepared materials in nitrophenol reduction at room temperature, a series of reusability tests were carried out on the best catalyst of the series (Au/AC_PVA-60), compared with material prepared using the commercial polymer (Au/AC_PVA-88). The catalytic performances were evaluated by comparing the conversion reached after a specific time (300 s) of the four recycling tests (Figure 7). The activity slightly decreased during the cycles, but in general, no differences were observed in terms of apparent kinetic constant.

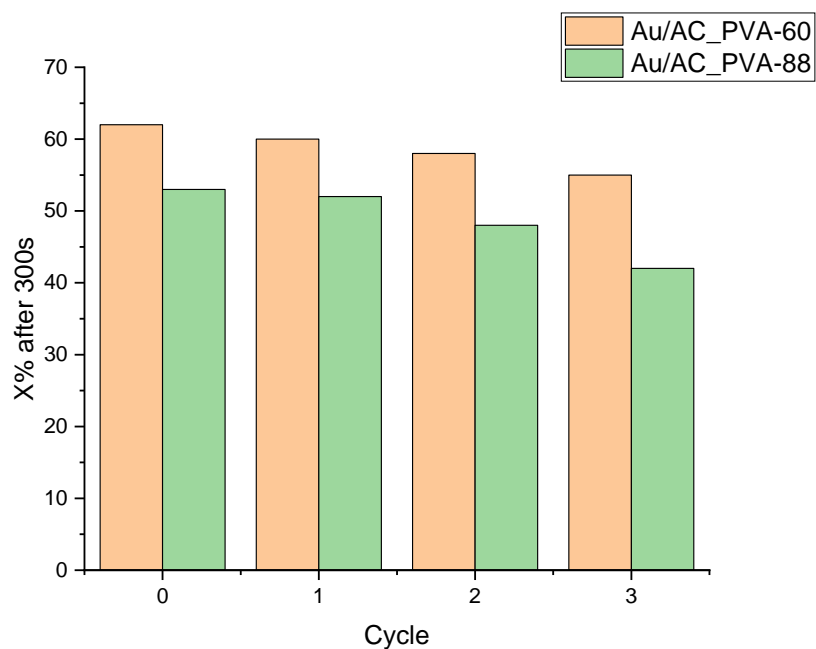


Figure 7. Reusability tests on 4-NP reduction using two catalysts prepared with either a synthesized or a commercial polymer.

2.4. Characterization of Au Colloidal Nanoparticles for Evaluating the Difference in Catalytic Activity of the Two Reactions Presented

In order to understand whether the different catalytic behavior displayed by the studied catalysts depends on an intrinsically different activity of the gold nanoparticles or on a secondary effect induced by the different reaction temperature (25 °C for 4-NP reduction and 70 °C for HMF oxidation), further characterization was carried out on the Au colloidal solution without the presence of support, before the deposition on the support, to exclude possible metal–support interaction effects during the immobilization step. For this study, the polymer that induced the greatest difference between the two catalytic performances was used (HD = 99%). The as-prepared Au NPs suspension was characterized by means of both DLS and ELS, before the addition of the support. In either case, the analysis was conducted gradually increasing the temperature from 25 °C to 70 °C and then was lowered again to 25 °C.

From the results presented in Figure 8, it is possible to observe that above 50 °C, there was a sharp decrease in DLS diameter, as well as a drop in the absolute value of the ζ -potential. It is also possible to observe that there was a very noticeable difference between the heating and the cooling ramps—namely, the DLS diameter was lower, and the absolute value of the ζ -potential was almost double. This suggests that a change occurred on the surface of the Au colloidal nanoparticles during the heating process. In particular, a detachment of the PVA from the surface of the nanoparticle would explain the lower DLS diameter, and the removal of a steric stabilizing agent could give way to a higher degree of electrostatic stabilization from the ions present in the solution, which would explain the higher absolute value of the ζ -potential.

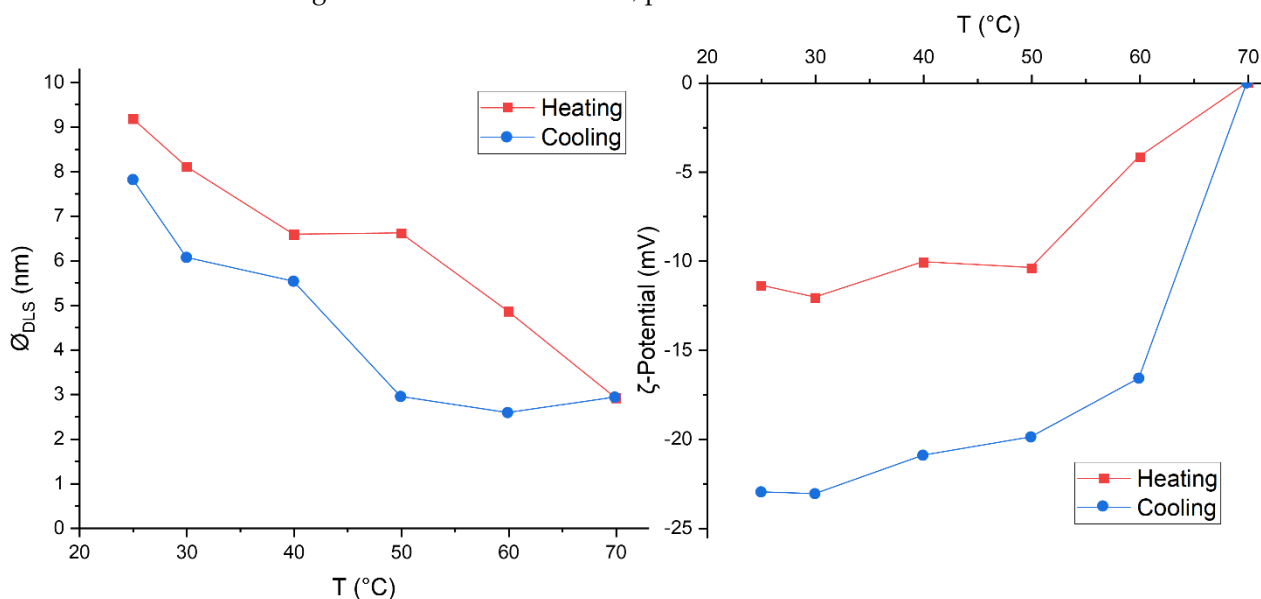


Figure 8. Effect of temperature on DLS diameter (left) and ζ -Potential measured via ELS (right) of Au-PVA_99 colloidal suspension during heating (red curves) and cooling (blue curves).

2.5. Effect of Polymer Removal

Based on the promising DLS results for the Au colloidal nanoparticles, and to better evaluate the observed trend, the Au/AC sample that displayed the greatest difference in performance between the two reactions (HD = 99%) was washed on a Büchner filter with distilled water at 60 °C to remove the capping agent from the surface of the nanoparticles [48]. The washed catalyst did not display a significant improvement in terms of catalytic performance regarding HMF oxidation (Figure 9), supporting the hypothesis that most of the polymer is removed during the reaction. The slight improvement in FDCA selectivity might be explained by the fact that removing PVA before the reaction allowed the catalyst to be fully active from the very first moments of the reaction. The washing

process seemed to be of little impact on the catalytic performances regarding HMF oxidation. However, the catalytic performance in 4-NP reduction significantly improved. The apparent kinetic constant increased from 0.0018 min^{-1} to 0.2897 min^{-1} , a much higher value than the best performance obtained with any of the unwashed catalysts.

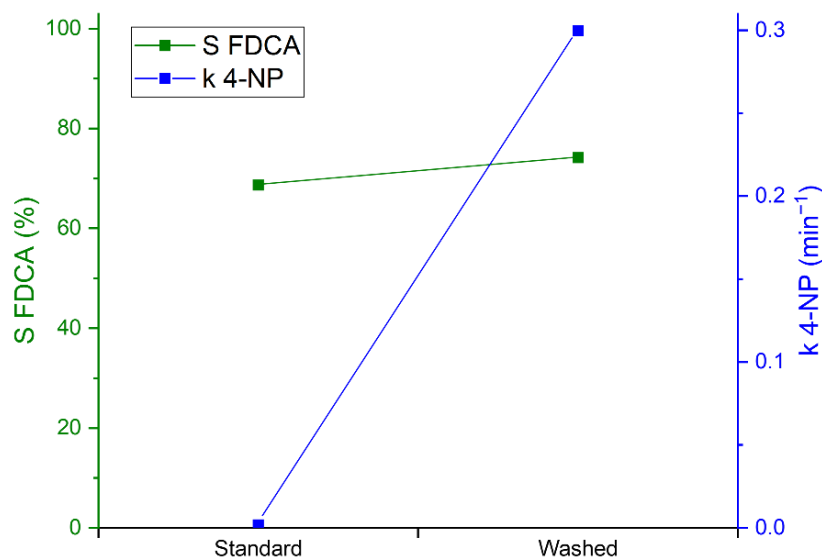


Figure 9. Comparison of the catalytic performances of standard and washed catalysts (HD = 99%) in terms of FDCA selectivity (in green) and 4-NP reduction apparent kinetic constant (in blue).

Considering these results, the catalysts were tested once again in the reduction of 4-NP but at the same temperature used for HMF oxidation ($70 \text{ }^\circ\text{C}$). The results reported in Figure 10 show the expected increase in kinetic constant caused by the higher reaction temperature used. This increase was, however, uneven across the different hydrolysis degrees. The samples that displayed the worst catalytic performances at $25 \text{ }^\circ\text{C}$ were the ones that improved their catalytic performances the most at a higher reaction temperature. Interestingly, the variation in apparent kinetic constant at $70 \text{ }^\circ\text{C}$ with the hydrolysis degree was very closely correlated with the mean Au particle size from TEM analysis. This correlation reinforced the idea that the catalytic activity at low reaction temperatures is severely hindered by the polymeric shell around the nanoparticles, and that hot water is able to solubilize PVA, detaching it from the nanoparticles and thus improving the overall catalytic performance, which is in agreement with previous results indicating that in reactions that occur at lower reaction temperatures below $30 \text{ }^\circ\text{C}$, the impact is more significant [48]. The presence of stabilizer on the surface of the catalysts still has an unclear role, it can improve catalytic performance, or it can be detrimental depending on the nature of the reaction and experimental conditions used [49]. In this case, the presence of PVA had a negative effect on the overall activity for reactions carried out at a low reaction temperature; the steric nature of the stabilizing agent probably partially blocked the active sites of the catalyst. This hypothesis has been confirmed in research conducted by Yang et al., which demonstrates that the polymer presence on gold nanoparticles can sterically inhibit the reactivity of Au/TiO₂ catalysts in CO oxidation [50].

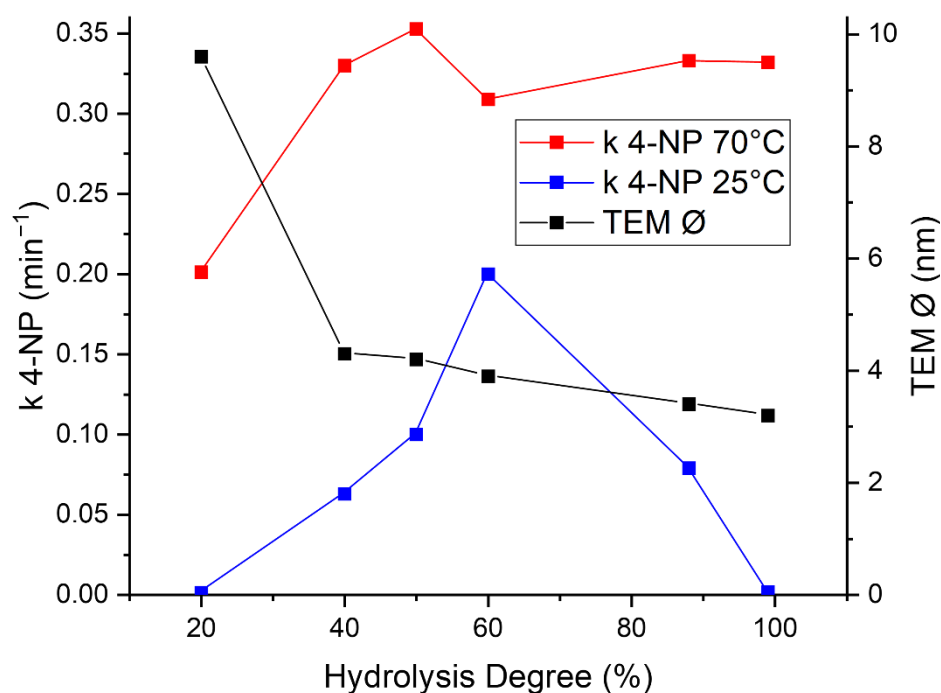


Figure 10. Effect of temperature on the catalytic performances in 4-NP reduction. Blue indicates the apparent kinetic constants at 25 °C; red indicates the apparent kinetic constants at 70 °C; black indicates the mean Au particle sizes measured with TEM analysis of the fresh catalysts.

2.6. Titania-Supported Catalysts

To confirm the general application of our hypothesis and exclude the effect of the activated carbon, colloidal Au nanoparticles supported on titania were prepared using the same polymeric stabilizers (PVA-99) employed in the previous tests and subsequently washed with hot water (e.g., 90 °C) to remove the organic coating. The materials washed and unwashed were tested in the reactions chosen, and the catalytic activity was compared. Based on the results obtained, the trend observed for the activated carbon-supported catalysts was confirmed (Figure 11). An improvement in the catalytic activity in terms of kinetic constant and conversion could be detected by employing treated Au/TiO₂ in the 4-nitrophenol reduction, during which the kinetic constant changed from 0.025 to 0.1 min⁻¹. Analogous results were observed when comparing the FDCA selectivity in the washed and unwashed samples (Table 2). In general, it could be hypothesized that varying the reaction conditions changes the behavior and fate of PVA on the surface of the nanoparticles, thus inducing a significant change in the reaction outcome.

To further investigate how the reaction conditions can change the catalytic behavior of the synthesized nanomaterials, several tests were carried out using activated-carbon- and titania-supported catalysts washed and unwashed at different temperatures (25 and 70 °C) (Figure 12). In the case of reaction at 25 °C, different catalytic performances were observed in the kinetic curves between the treated and untreated systems, in agreement with the data previously described. In comparison, both samples employed at 70 °C exhibited similar catalytic activities, confirming the temperature-dependent activity of the prepared catalysts, due to the detachment of polymeric stabilizers during the reaction, which can lead to a restructuring of the surface of the catalyst and therefore can affect the availability of active sites.

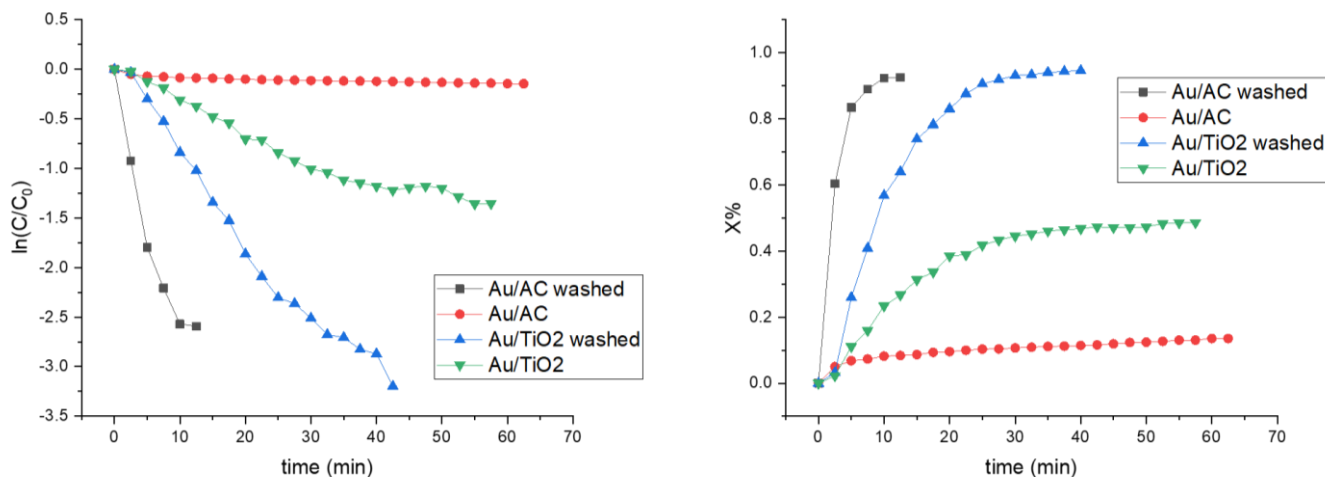


Figure 11. Kinetic performances in 4-NP reduction with the washed and unwashed catalysts prepared using different supports (active carbon and titania).

Table 2. Kinetic data for gold nanocatalysts washed and unwashed supported on activated carbon and titania.

Sample	4-NP (25 °C)		HMF (70 °C)			
	k_{app} (min ⁻¹)	X _{4-NP} (%)	X HMF (%)	S HMFCA (%)	S FFCA (%)	S FDCA (%)
Au/AC_PVA-99	$1.8 \times 10^{-3} \pm 4 \times 10^{-4}$	16 ± 0.2	100	31	0	69
Au/AC_PVA-99-W	$0.3 \pm 3 \times 10^{-2}$	99 ± 1	100	26	0	74
Au/TiO ₂ _PVA-99	$2.5 \times 10^{-2} \pm 1 \times 10^{-3}$	48 ± 1	100	59	1	40
Au/TiO ₂ _PVA-99-W	$0.1 \pm 3 \times 10^{-3}$	99 ± 1	100	54	1	45

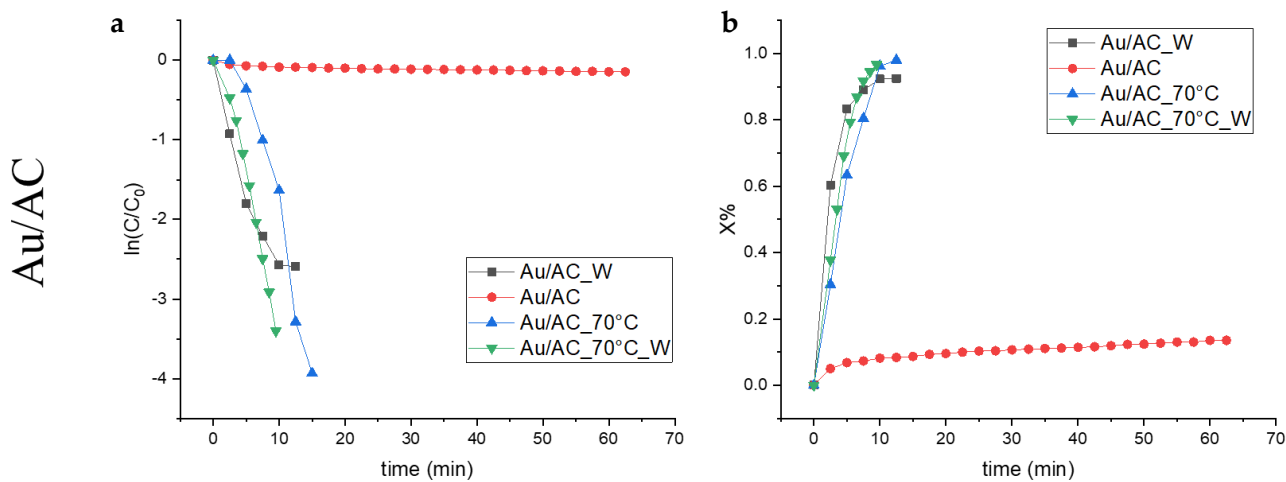


Figure 12. Cont.

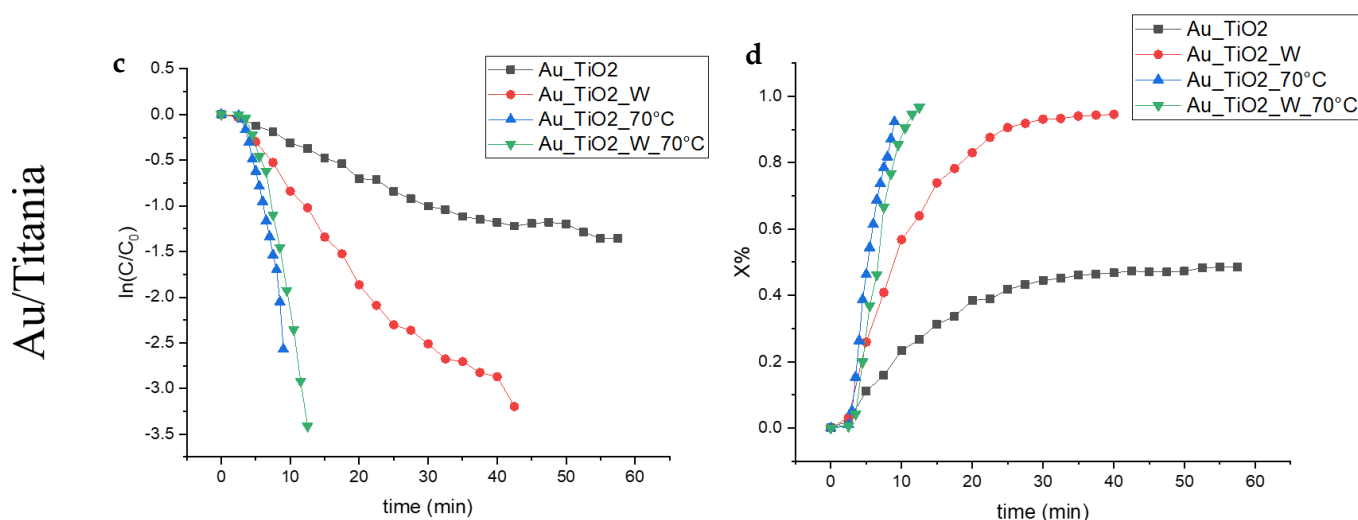


Figure 12. Kinetic performances in 4-NP reduction of the washed and unwashed catalysts supported on either active carbon (a,b) above) or titania (c,d) at room temperature and at 70 °C.

2.7. Characterization of the Washed Catalysts

The prepared catalysts were characterized by spectroscopic (ATR-IR and XPS) and microscopy analysis (TEM) in order to rationalize the behavior observed during the catalytic tests. Specifically, the techniques were chosen to investigate the effect of the treatment with hot water on the surface of catalysts and mean Au particle size. The IR spectra of gold nanoparticles supported on titania after the washing is reported in Figure 5 and compared with the same sample untreated and titania. The O–H stretching and bending at 3300 and 1650 cm^{-1} , respectively, were ascribed to the water adsorbed on the surface of the catalyst. Despite the presence of the intense band derived from water, in the nanostructured catalysts (Au/TiO₂), the presence of C–H stretching at 3000 cm^{-1} and the signal of C–H bending at 1300 cm^{-1} of the aliphatic polymeric chains were observed (Figure 13). The disappearance of this band in the washed sample confirmed the removal of the polymer from the surface of the catalysts with the methodology proposed. In addition, the trend highlighted was further investigated by XPS analysis through the comparison of the active phase expose before and after the washing phase (Table 3, Figure S1). As expected, the typical XPS spectrum related to the gold metallic state could be observed in the two peaks at 84 eV and 87.5 eV attributed to the Au 4f_{7/2} and Au 4f_{5/2} spin-orbital coupling, respectively. However, in the case of catalysts supported on titania a shift of Au 4f binding, energy was observed due to the dominant presence of Au^{δ−} (83.2 eV) on the support that can interact with the superficial Ti³⁺ defective sites [51–53]. Instead, the Ti exhibited two binding energies peaks at 458 eV and 464 eV related to Ti 2p_{3/2} and Ti 2p_{1/2} electrons, respectively [54,55]. By the comparison between the samples washed and unwashed, increased exposure of gold was observed from 0.03 to 0.06. In the case of active carbon-supported materials, Au/AC ratio changed slightly from 0.02 to 0.03.

However, regarding the percentage of C on the surface, a decrement of 3% was obtained, which provided evidence of PVA detachment during the washing phase. More significant results were obtained for the Au/TiO₂ catalysts, where the Au/Ti ratio increased from 0.03 to 0.06, confirming the IR results. Moreover, the unchanged C percentages could be derived from the adsorbed carbon dioxide on the catalyst surface, in line with the results from Mohite et al. [54]. The acquisition of TEM images allowed the evaluation of the effect of the treatment on the size of Au nanoparticles. By the employment of hot water to remove the polymeric stabilizer, the dimension of gold nanoparticles did not change in the activated carbon-supported catalysts, and therefore, the presence of large sintering phenomena was excluded (Figures S2 and S3). In comparison, a slight but not significant increase in nanoparticles size was observed in the Au/TiO₂ materials after

washing. The images acquired confirmed that the AuNPs dimension remained constant when the samples were treated to remove the organic coating.

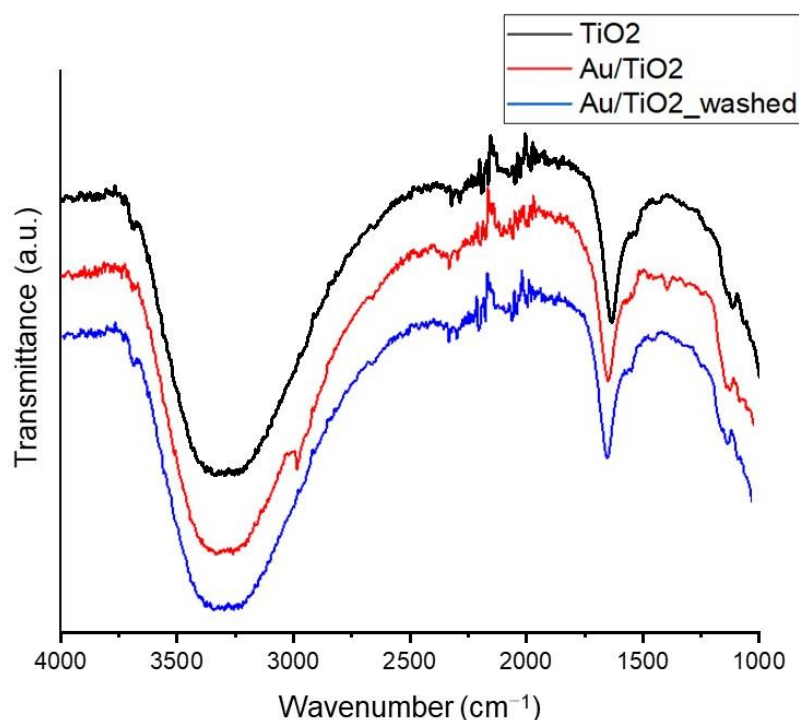


Figure 13. IR spectra of TiO₂, Au/TiO₂, and Au/TiO₂ catalysts after the treatment with hot water.

Table 3. XPS data for the catalysts treated and untreated supported on activated carbon and titania.

Sample	BE Au 4f 7/2 (eV)	Surface Au (%)	Surface C (%)	Surface Ti (%)	Au/Ti
Au/AC_PVA-99	84.1	1.47	91.2	-	0.02
Au/AC_PVA-99-w	84.1	2.34	88.2	-	0.03
Au/TiO ₂ _PVA-99	83.2	0.68	22.0	22.7	0.03
Au/TiO ₂ _PVA-99-w	83.2	1.26	22.0	22.0	0.06

3. Materials and Methods

3.1. Materials

Tetrachlorauric acid (HAuCl₄·3H₂O), sodium borohydride (NaBH₄, 99%), activated carbon NORIT SX1G, Titania P-25, sulfuric acid (H₂SO₄, 96%), 4-nitrophenol (>99%), and polyvinyl alcohol (Mw: 13,000–23,000) with different hydrolysis degrees (98–99% and 88%), as well as the HMF oxidation standards used for the analysis (HMFCA, FFCA, and FDCA), were purchased from Sigma Aldrich (Milan, Italy), and 5-hydroxymethylfurfural was purchased from AVA Biochem (Zug, Switzerland). The polymeric stabilizers were synthesized by free-radical polymerization of the vinyl-acetate and subsequent, controlled saponification was followed to obtain the polyvinyl alcohol with different hydrolysis degrees following the methodologies described in a previous study [41]. The solvents were used without further processes of purification.

3.2. Catalysts Preparation

A typical experimental protocol for the synthesized Au–PVA catalysts is the following: A colloidal gold solution was prepared by dissolving 0.76 g (1.9 mmol) of HAuCl₄·3H₂O in 200 mL of distilled H₂O. Subsequently, 5.5 mL were withdrawn from the initial solution and diluted in 385 mL of distilled H₂O, to which a volume of 1% w/w polymer aqueous solution was added to obtain the desired Au:PVA weight ratio. After 3 min, a freshly prepared aqueous solution of NaBH₄ (Au:NaBH₄ = 1:5 mol/mol) was added, and a red

Au⁰ sol was immediately formed. The colloidal solution was stirred for 30 min and, finally, the Au colloidal nanoparticles were immobilized by adding the support (activated carbon, AC) under vigorous stirring. The solution was acidified at pH 2 by using sulfuric acid and was stirred for 1 h at room temperature. In the case of nanoparticles supported on titania, the pH of the solution was not changed, in agreement with its isoelectric point, and the mixture was stirred for 4 h to have a complete immobilization. The extent of support was calculated in order to have a nominal metal loading of 1 wt.%. Finally, the catalyst was filtered using a Buchner funnel and washed several times with distilled water to remove ionic species and mother liquors, until a neutral pH was reached. After drying overnight at room temperature, the solids were dried at 80 °C in an oven for 4 h in static air conditions. The colloidal solution was characterized by means of UV–Vis spectroscopy, dynamic light scattering (DLS), and electrophoretic light scattering (ELS). The supported catalysts were characterized using X-ray photoelectron spectroscopy (XPS), transmission electron microscopy (TEM), and X-ray diffraction (XRD), and for titania supported catalysts, also by infrared spectroscopy (IR) [41].

3.3. Characterization

Colloidal solutions were characterized by dynamic light scattering (DLS) and electrophoretic light scattering (ELS) measures, registered by using a Malvern Panalytical (Malvern, United Kingdom) Zetasizer Nano ZS instrument. The particle size distribution was carried out using a standard polystyrene cell at 25 °C, while for the zeta potential analysis and for the investigation of the stability of the colloid by changing the temperature, a capillary polycarbonate cell equipped with electrodes was employed. Infrared spectra (FT-IR) were acquired through an ATR-IR Bruker (Billerica, MA, USA) Alpha I spectrometer in order to characterize the supported Au/TiO₂ nanoparticles, using 64 scans to enhance the signal-to-noise ratio of the spectra. Transmission electron microscopy (TEM) images were obtained using a Thermo Fisher (Waltham, MA, USA) FEI Talos F200x high-resolution transmission microscope (Thermo Fisher Scientific, Waltham, MA, USA) to elucidate the morphology and dispersion of the active phase. Samples were suspended in ethanol and treated by ultrasound for 15 min. A drop of the suspension was deposited on “quantifoil-carbon film” supported on a Cu grid and dried before analysis. TEM images were processed by using ImageJ. 300–400 NPs were measured for each sample, using different areas of the sample analyzed. X-ray photoelectron spectroscopy (XPS) spectra were recorded on a PHI (Chanhassen, MN, USA) Versa Probe II physical electronic spectrometer using monochromatic Al K radiation (52.8 W, 15 kV, 1486.6 eV) and a dual-beam charge neutralizer for analyzing the core-level signals of the elements of interest with a hemispherical multichannel detector. The XPS spectra of the samples were recorded with a constant pass energy value at 29.35 eV and a beam diameter of 100 μm. The energy scale was calibrated using Cu 2p_{3/2}, Ag 3d_{5/2}, and Au 4f_{7/2} photoelectron lines at 932.7, 368.2, and 83.95 eV, respectively. The X-ray photoelectron spectra obtained were analyzed using PHI SmartSoft (VersaProbe 4, Chanhassen, MN, USA) software and processed using the MultiPak 9.6.0.15 package. The binding energy values were referenced to C 1s signal at 284.5 eV. Shirley-type background and Gauss–Lorentz curves were used to determine the binding energies. Atomic concentration percentages of the characteristic elements were determined considering the corresponding area sensitivity factor for the different measured spectral regions. Powder X-ray diffraction (XRD) patterns and calculation of the mean Au crystallite size were reported in the previous paper by employing a Malvern Panalytical (Malvern, United Kingdom) X’PertPRO X-ray diffractometer using a Cu radiation source (1.54 Å) [41].

3.4. Catalytic Tests

3.4.1. 5-Hydroxymethylfurfural Oxidation Test

HMF oxidation tests were conducted out in a 100 mL PARR autoclave. Standard reactions were carried out in the following conditions: HMF: Au: NaOH molar ratios of

1:0.01:4 at 70 °C, 4 h of reaction time from the moment the reaction temperature was reached, with 10 bar of O₂, 600 rpm stirring. After each reaction, the catalyst was removed via centrifugation, and the clear solution was diluted 1:5 before being injected in HPLC were carried out in an Agilent 1260 Infinity instrument equipped with a BioRAD Aminex HPX-87H column and a DAD detector. For each species present in the reaction pathway (HMF, HMFCFA, FFCA, and FDCA), an external calibration curve was used to calculate their respective concentration.

3.4.2. 4-Nitrophenol Calibration Test

To set up the UV–Vis experiments the extinction coefficient was calculated by preparing five solutions of different 4-NP concentrations (1.5×10^{-4} M, 1.0×10^{-4} M, 5.0×10^{-4} M, 2.5×10^{-5} M, 1.0×10^{-4} M) and 4.5×10^{-4} M in NaBH₄ using an in situ Agilent Cary 3500 UV–Vis Spectrometer equipped with 1 cm path cuvette. In agreement with the literature, the average extinction coefficient derived from the calibration curves repeated three times is $18,900 \text{ M}^{-1} \text{ cm}^{-1}$ [56,57].

3.4.3. Catalytic Reduction of 4-Nitrophenol

The catalytic 4-nitrophenol reduction with NaBH₄ was employed as a model reaction to investigate the effect of the polymeric stabilizers and the influence of the reaction temperature on the catalytic performances. The reaction was carried out in an aqueous phase under mild conditions of pressure and temperature (25 °C). The standard reaction was accomplished by preparing 4-NP aqueous solutions (2.0×10^{-4} M) in a 25 mL volumetric flask. Then, a fresh solution of NaBH₄ (9.0×10^{-4} M) in 25 mL was prepared with a molar ratio of 4-NP:NaBH₄ of 1:45 mol/mol in order to uphold a pseudo-first-order kinetic model. Moreover, reference NaBH₄ solution in a 25 mL (4.5×10^{-4} M) for the UV–Vis measurements was prepared. The following experimental protocol was used: The catalyst (4 mg) was first added inside a beaker, and then the 4-NP solution was added. Immediately after, 25 mL of NaBH₄ solution (9.0×10^{-4} M) was added and this time was considered the starting of the reaction. After mixing, an aliquot was withdrawn from the beaker and poured in a quartz cuvette, and then subsequently inserted in the UV–Vis spectrometer's stage. After the NaBH₄ addition, 2.5 min were passed as induction time before starting the measurement. The optical absorbance of the reaction was set to be automatically evaluated every 2.5 min for 25 cycles to measure the decrease in 4-nitrophenol concentration as a function of reaction time. The tests carried out at different temperature was accomplished using the same experimental setup described, but different temperatures were set by the instrument software.

4. Conclusions

The effects of PVA with different hydrolysis degrees on the catalytic performance of supported gold nanoparticles, as well as the temperature-dependence activity, were investigated. To this end, 4-NP reduction and HMF oxidation were employed to evaluate the influence of polymeric stabilizers and reaction temperature. In particular, correlating the hydrolysis with the 4-NP's apparent kinetic constant and FDCA selectivity related to HMF reaction, volcano shape plots were obtained for both reactions in which the maximum of the curves was represented for the samples prepared using PVA with intermediate values of hydrolysis. The obtained results were in agreement with the percentage of gold exposure and the size of the Au nanoparticles. However, different behavior between the two reactions in terms of catalytic activity was observed for a sample called Au/AC_PVA-99. For this reason, the HMF reaction conditions were simulated in the 4-NP reaction to investigate the role of the polymeric stabilizers by increasing reaction temperature. The obtained curve highlighted how the temperature led to an increase in the kinetic activity for all samples; therefore, a correlation with the TEM diameters allowed us to establish a direct size–activity correlation. This observation was also supported by DLS and ELS analysis carried out at different temperatures to monitor the changing of hydrodynamic

volume and superficial charge of the samples. To further investigate the phenomena, the catalyst was treated with hot water (60 °C) in order to remove the organic coating and was tested in the two redox reactions chosen. For the 4-NP, a significant difference was observed from the untreated samples, whereas for HMF, the same behavior was obtained. In this way, the detachment of the polymeric stabilizer due to the upper reaction temperature was confirmed. To exclude the effect of activated carbon, titania-supported gold nanocatalysts were prepared, and in this case, the same trend as the one previously described was observed. In the study reported in this paper, we emphasized the effect of the polymeric stabilizers in gold nanocatalysts for the redox reactions and the modification of the temperature reaction can change the PVA behavior on the catalyst surface and therefore influence the catalytic outcomes.

Supplementary Materials: The following supporting information can be downloaded at: <https://www.mdpi.com/article/10.3390/catal12030323/s1>, Figure S1: XPS spectra for Au/AC_PVA-99-w (a), Au/TiO₂_PVA-99 (b) and Au/TiO₂_PVA-99-w (c), Figure S2: TEM images of treated and untreated catalysts supported on active carbon and titania, Figure S3: Particles size distribution of treated and untreated catalysts supported on active carbon and titania, Table S1: Catalytic results on the HMF oxidation reaction, Table S2: Kinetic parameters (apparent rate constants and conversion) for the 4-nitrophenol reduction related to catalysts prepared using PVA with different hydrolysis degrees.

Author Contributions: Conceptualization, S.S., S.A., N.D. and D.C.; data curation, S.S., A.A., F.L. and J.A.C.; formal analysis, E.R.-A. and J.A.C.; investigation, A.A. and F.L.; methodology, S.S., A.A. and F.L.; project administration, S.A., D.C. and N.D.; supervision, J.A.C., S.A., D.C. and N.D.; validation, A.A., F.L. and E.R.-A.; visualization, S.S. and E.R.-A.; writing—original draft preparation, S.A., D.C. and N.D.; writing—review and editing, S.S., A.A., F.L., E.R.-A., J.A.C., S.A., D.C. and N.D. All authors have read and agreed to the published version of the manuscript.

Funding: This research received no external funding.

Data Availability Statement: Data are contained within the article.

Acknowledgments: The authors thank the anonymous reviewers for their constructive comments.

Conflicts of Interest: The authors declare no conflict of interest.

References

1. Rogers, C.; Perkins, W.S.; Veber, G.; Williams, T.E.; Cloke, R.R.; Fischer, F.R. Synergistic Enhancement of Electrocatalytic CO₂ Reduction with Gold Nanoparticles Embedded in Functional Graphene Nanoribbon Composite Electrodes. *J. Am. Chem. Soc.* **2017**, *139*, 4052–4061. [[CrossRef](#)] [[PubMed](#)]
2. Torres Galvis, H.M.; Bitter, J.H.; Khare, C.B.; Ruitenbeek, M.; Dugulan, A.I.; de Jong, K.P. Supported Iron Nanoparticles as Catalysts for Sustainable Production of Lower Olefins. *Science* **2012**, *335*, 835–838. [[CrossRef](#)] [[PubMed](#)]
3. Gandarias, I.; Miedziak, P.J.; Nowicka, E.; Douthwaite, M.; Morgan, D.J.; Hutchings, G.J.; Taylor, S.H. Selective Oxidation of N-Butanol Using Gold-Palladium Supported Nanoparticles Under Base-Free Conditions. *ChemSusChem* **2015**, *8*, 473–480. [[CrossRef](#)] [[PubMed](#)]
4. Tada, H. Overall Water Splitting and Hydrogen Peroxide Synthesis by Gold Nanoparticle-Based Plasmonic Photocatalysts. *Nanoscale Adv.* **2019**, *1*, 4238–4245. [[CrossRef](#)]
5. Whipple, D.T.; Kenis, P.J.A. Prospects of CO₂ Utilization via Direct Heterogeneous Electrochemical Reduction. *J. Phys. Chem. Lett.* **2010**, *1*, 3451–3458. [[CrossRef](#)]
6. Hall, A.S.; Yoon, Y.; Wuttig, A.; Surendranath, Y. Mesostructure-Induced Selectivity in CO₂ Reduction Catalysis. *J. Am. Chem. Soc.* **2015**, *137*, 14834–14837. [[CrossRef](#)]
7. Zhang, H.; Wang, C.; Sun, H.-L.; Fu, G.; Chen, S.; Zhang, Y.-J.; Chen, B.-H.; Anema, J.R.; Yang, Z.-L.; Li, J.-F.; et al. In Situ Dynamic Tracking of Heterogeneous Nanocatalytic Processes by Shell-Isolated Nanoparticle-Enhanced Raman Spectroscopy. *Nat. Commun.* **2017**, *8*, 15447. [[CrossRef](#)]
8. Hafeez, S.; Sanchez, F.; Al-Salem, S.M.; Villa, A.; Manos, G.; Dimitratos, N.; Constantinou, A. Decomposition of Additive-Free Formic Acid Using a Pd/C Catalyst in Flow: Experimental and CFD Modelling Studies. *Catalysts* **2021**, *11*, 341. [[CrossRef](#)]
9. Ndolomingo, M.J.; Bingwa, N.; Meijboom, R. Review of Supported Metal Nanoparticles: Synthesis Methodologies, Advantages and Application as Catalysts. *J. Mater. Sci.* **2020**, *55*, 6195–6241. [[CrossRef](#)]
10. Hsieh, B.-J.; Tsai, M.-C.; Pan, C.-J.; Su, W.-N.; Rick, J.; Chou, H.-L.; Lee, J.-F.; Hwang, B.-J. Tuning Metal Support Interactions Enhances the Activity and Durability of TiO₂-Supported Pt Nanocatalysts. *Electrochim. Acta* **2017**, *224*, 452–459. [[CrossRef](#)]

11. Chen, S.; Abdel-Mageed, A.M.; Gauckler, C.; Olesen, S.E.; Chorkendorff, I.; Behm, R.J. Selective CO Methanation on Isostructural Ru Nanocatalysts: The Role of Support Effects. *J. Catal.* **2019**, *373*, 103–115. [[CrossRef](#)]
12. Ferrando, R.; Jellinek, J.; Johnston, R.L. Nanoalloys: From Theory to Applications of Alloy Clusters and Nanoparticles. *Chem. Rev.* **2008**, *108*, 845–910. [[CrossRef](#)] [[PubMed](#)]
13. Iben Ayad, A.; Luart, D.; Ould Dris, A.; Guénin, E. Kinetic Analysis of 4-Nitrophenol Reduction by “Water-Soluble” Palladium Nanoparticles. *Nanomaterials* **2020**, *10*, 1169. [[CrossRef](#)]
14. Daraee, H.; Eatemadi, A.; Abbasi, E.; Fekri Aval, S.; Kouhi, M.; Akbarzadeh, A. Application of Gold Nanoparticles in Biomedical and Drug Delivery. *Artif. Cells Nanomed. Biotechnol.* **2016**, *44*, 410–422. [[CrossRef](#)]
15. Bingwa, N.; Patala, R.; Noh, J.-H.; Ndolomingo, M.J.; Tetyana, S.; Bewana, S.; Meijboom, R. Synergistic Effects of Gold–Palladium Nanoalloys and Reducible Supports on the Catalytic Reduction of 4-Nitrophenol. *Langmuir* **2017**, *33*, 7086–7095. [[CrossRef](#)]
16. Vial, S.; Reis, R.L.; Oliveira, J.M. Recent Advances Using Gold Nanoparticles as a Promising Multimodal Tool for Tissue Engineering and Regenerative Medicine. *Curr. Opin. Solid State Mater. Sci.* **2017**, *21*, 92–112. [[CrossRef](#)]
17. Jin, L.; Liu, B.; Duay, S.; He, J. Engineering Surface Ligands of Noble Metal Nanocatalysts in Tuning the Product Selectivity. *Catalysts* **2017**, *7*, 44. [[CrossRef](#)]
18. Narayanan, R.; El-Sayed, M.A. Shape-Dependent Catalytic Activity of Platinum Nanoparticles in Colloidal Solution. *Nano Lett.* **2004**, *4*, 1343–1348. [[CrossRef](#)]
19. Tian, N.; Zhou, Z.-Y.; Sun, S.-G.; Ding, Y.; Wang, Z.L. Synthesis of Tetrahedral Platinum Nanocrystals with High-Index Facets and High Electro-Oxidation Activity. *Science* **2007**, *316*, 732–735. [[CrossRef](#)]
20. Nanda, K.K. Size-Dependent Density of Nanoparticles and Nanostructured Materials. *Phys. Lett. A* **2012**, *376*, 3301–3302. [[CrossRef](#)]
21. Lim, D.C.; Lopez-Salido, I.; Dietsche, R.; Bubek, M.; Kim, Y.D. Size-Selectivity in the Oxidation Behaviors of Au Nanoparticles. *Angew. Chem. Int. Ed.* **2006**, *45*, 2413–2415. [[CrossRef](#)] [[PubMed](#)]
22. Megías-Sayago, C.; Lolli, A.; Bonincontro, D.; Penkova, A.; Albonetti, S.; Cavani, F.; Odriozola, J.A.; Ivanova, S. Effect of Gold Particles Size over Au/C Catalyst Selectivity in HMF Oxidation Reaction. *ChemCatChem* **2020**, *12*, 1177–1183. [[CrossRef](#)]
23. Fritz, G.; Schädler, V.; Willenbacher, N.; Wagner, N.J. Electrosteric Stabilization of Colloidal Dispersions. *Langmuir* **2002**, *18*, 6381–6390. [[CrossRef](#)]
24. Polte, J. Fundamental Growth Principles of Colloidal Metal Nanoparticles—A New Perspective. *CrystEngComm* **2015**, *17*, 6809–6830. [[CrossRef](#)]
25. Rossi, L.M.; Fiorio, J.L.; Garcia, M.A.S.; Ferraz, C.P. The Role and Fate of Capping Ligands in Colloidally Prepared Metal Nanoparticle Catalysts. *Dalton Trans.* **2018**, *47*, 5889–5915. [[CrossRef](#)]
26. Ansar, S.M.; Kitchens, C.L. Impact of Gold Nanoparticle Stabilizing Ligands on the Colloidal Catalytic Reduction of 4-Nitrophenol. *ACS Catal.* **2016**, *6*, 5553–5560. [[CrossRef](#)]
27. Zhao, Y.; Baeza, J.A.; Koteswara Rao, N.; Calvo, L.; Gilarranz, M.A.; Li, Y.D.; Lefferts, L. Unsupported PVA- and PVP-Stabilized Pd Nanoparticles as Catalyst for Nitrite Hydrogenation in Aqueous Phase. *J. Catal.* **2014**, *318*, 162–169. [[CrossRef](#)]
28. Thiele, H.; von Lavern, H.S. Synthetic Protective Colloids. *J. Colloid Sci.* **1965**, *20*, 679–694. [[CrossRef](#)]
29. Singh, M.; Sinha, I.; Premkumar, M.; Singh, A.K.; Mandal, R.K. Structural and Surface Plasmon Behavior of Cu Nanoparticles Using Different Stabilizers. *Colloids Surf. A Physicochem. Eng. Asp.* **2010**, *359*, 88–94. [[CrossRef](#)]
30. Abis, L.; Dimitritatos, N.; Sankar, M.; Freakley, S.J.; Hutchings, G.J. The Effect of Polymer Addition on Base Catalyzed Glycerol Oxidation Using Gold and Gold–Palladium Bimetallic Catalysts. *Top. Catal.* **2020**, *63*, 394–402. [[CrossRef](#)]
31. Kim, E.J.; Yeum, J.H.; Choi, J.H. Effects of Polymeric Stabilizers on the Synthesis of Gold Nanoparticles. *J. Mater. Sci. Technol.* **2014**, *30*, 107–111. [[CrossRef](#)]
32. Chen, G.; Xu, C.; Huang, X.; Ye, J.; Gu, L.; Li, G.; Tang, Z.; Wu, B.; Yang, H.; Zhao, Z.; et al. Interfacial Electronic Effects Control the Reaction Selectivity of Platinum Catalysts. *Nat. Mater.* **2016**, *15*, 564–569. [[CrossRef](#)] [[PubMed](#)]
33. Zhang, P.; Sham, T.K. Tuning the Electronic Behavior of Au Nanoparticles with Capping Molecules. *Appl. Phys. Lett.* **2002**, *81*, 736–738. [[CrossRef](#)]
34. Schäfer, C.; Mhadgut, S.C.; Kugyela, N.; Török, M.; Török, B. Proline-Induced Enantioselective Heterogeneous Catalytic Hydrogenation of Isophorone on Basic Polymer-Supported Pd Catalysts. *Catal. Sci. Technol.* **2015**, *5*, 716–723. [[CrossRef](#)]
35. Liu, J.; Bai, P.; Zhao, X.S. Ruthenium Nanoparticles Embedded in Mesoporous Carbon Microfibers: Preparation, Characterization and Catalytic Properties in the Hydrogenation of d-Glucose. *Phys. Chem. Chem. Phys.* **2011**, *13*, 3758–3763. [[CrossRef](#)]
36. Albonetti, S.; Lolli, A.; Morandi, V.; Migliori, A.; Lucarelli, C.; Cavani, F. Conversion of 5-Hydroxymethylfurfural to 2,5-Furandicarboxylic Acid over Au-Based Catalysts: Optimization of Active Phase and Metal–Support Interaction. *Appl. Catal. B Environ.* **2015**, *163*, 520–530. [[CrossRef](#)]
37. Lolli, A.; Albonetti, S.; Utili, L.; Amadori, R.; Ospitali, F.; Lucarelli, C.; Cavani, F. Insights into the Reaction Mechanism for 5-Hydroxymethylfurfural Oxidation to FDCA on Bimetallic Pd–Au Nanoparticles. *Appl. Catal. A Gen.* **2015**, *504*, 408–419. [[CrossRef](#)]
38. Li, X.; Xu, J.; Wang, F.; Gao, J.; Zhou, L.; Yang, G. Direct Oxidation of Toluene to Benzoic Acid with Molecular Oxygen over Manganese Oxides. *Catal. Lett.* **2006**, *108*, 137–140. [[CrossRef](#)]
39. Davis, S.E.; Houk, L.R.; Tamargo, E.C.; Datye, A.K.; Davis, R.J. Oxidation of 5-Hydroxymethylfurfural over Supported Pt, Pd and Au Catalysts. *Catal. Today* **2011**, *160*, 55–60. [[CrossRef](#)]

40. Van Putten, R.-J.; van der Waal, J.C.; de Jong, E.; Rasrendra, C.B.; Heeres, H.J.; de Vries, J.G. Hydroxymethylfurfural, A Versatile Platform Chemical Made from Renewable Resources. *Chem. Rev.* **2013**, *113*, 1499–1597. [[CrossRef](#)]
41. Scurti, S.; Monti, E.; Rodríguez-Aguado, E.; Caretti, D.; Cecilia, J.A.; Dimitratos, N. Effect of Polyvinyl Alcohol Ligands on Supported Gold Nano-Catalysts: Morphological and Kinetics Studies. *Nanomaterials* **2021**, *11*, 879. [[CrossRef](#)] [[PubMed](#)]
42. Albonetti, S.; Pasini, T.; Lolli, A.; Blosi, M.; Piccinini, M.; Dimitratos, N.; Lopez-Sanchez, J.A.; Morgan, D.J.; Carley, A.F.; Hutchings, G.J.; et al. Selective Oxidation of 5-Hydroxymethyl-2-Furfural over TiO₂-Supported Gold–Copper Catalysts Prepared from Preformed Nanoparticles: Effect of Au/Cu Ratio. *Catal. Today* **2012**, *195*, 120–126. [[CrossRef](#)]
43. Zhang, J.; Chen, G.; Guay, D.; Chaker, M.; Ma, D. Highly Active PtAu Alloy Nanoparticle Catalysts for the Reduction of 4-Nitrophenol. *Nanoscale* **2014**, *6*, 2125–2130. [[CrossRef](#)] [[PubMed](#)]
44. Shen, W.; Qu, Y.; Pei, X.; Li, S.; You, S.; Wang, J.; Zhang, Z.; Zhou, J. Catalytic Reduction of 4-Nitrophenol Using Gold Nanoparticles Biosynthesized by Cell-Free Extracts of *Aspergillus* Sp. WL-Au. *J. Hazard. Mater.* **2017**, *321*, 299–306. [[CrossRef](#)]
45. Aditya, T.; Jana, J.; Singh, N.K.; Pal, A.; Pal, T. Remarkable Facet Selective Reduction of 4-Nitrophenol by Morphologically Tailored (111) Faceted Cu₂O Nanocatalyst. *ACS Omega* **2017**, *2*, 1968–1984. [[CrossRef](#)] [[PubMed](#)]
46. Wunder, S.; Polzer, F.; Lu, Y.; Mei, Y.; Ballauff, M. Kinetic Analysis of Catalytic Reduction of 4-Nitrophenol by Metallic Nanoparticles Immobilized in Spherical Polyelectrolyte Brushes. *J. Phys. Chem. C* **2010**, *114*, 8814–8820. [[CrossRef](#)]
47. Gu, S.; Wunder, S.; Lu, Y.; Ballauff, M.; Fenger, R.; Rademann, K.; Jaquet, B.; Zaccone, A. Kinetic Analysis of the Catalytic Reduction of 4-Nitrophenol by Metallic Nanoparticles. *J. Phys. Chem. C* **2014**, *118*, 18618–18625. [[CrossRef](#)]
48. Lopez-Sanchez, J.A.; Dimitratos, N.; Hammond, C.; Brett, G.L.; Kesavan, L.; White, S.; Miedziak, P.; Tiruvalam, R.; Jenkins, R.L.; Carley, A.F.; et al. Facile Removal of Stabilizer-Ligands from Supported Gold Nanoparticles. *Nat. Chem.* **2011**, *3*, 551–556. [[CrossRef](#)]
49. Baker, L.R.; Kennedy, G.; Krier, J.M.; Van Spronsen, M.; Onorato, R.M.; Somorjai, G.A. The Role of an Organic Cap in Nanoparticle Catalysis: Reversible Restructuring of Carbonaceous Material Controls Catalytic Activity of Platinum Nanoparticles for Ethylene Hydrogenation and Methanol Oxidation. *Catal. Lett.* **2012**, *142*, 1286–1294. [[CrossRef](#)]
50. Yang, N.; Pattison, S.; Douthwaite, M.; Zeng, G.; Zhang, H.; Ma, J.; Hutchings, G.J. Influence of Stabilizers on the Performance of Au/TiO₂ Catalysts for CO Oxidation. *ACS Catal.* **2021**, *11*, 11607–11615. [[CrossRef](#)]
51. Zielińska-Jurek, A.; Kowalska, E.; Sobczak, J.W.; Lisowski, W.; Ohtani, B.; Zaleska, A. Preparation and Characterization of Monometallic (Au) and Bimetallic (Ag/Au) Modified-Titania Photocatalysts Activated by Visible Light. *Appl. Catal. B Environ.* **2011**, *101*, 504–514. [[CrossRef](#)]
52. Chen, M.; Goodman, D.W. Catalytically Active Gold: From Nanoparticles to Ultrathin Films. *Acc. Chem. Res.* **2006**, *39*, 739–746. [[CrossRef](#)] [[PubMed](#)]
53. Moma, J.A.; Scurrill, M.S.; Jordaan, W.A. Effects of Incorporation of Ions into Au/TiO₂ Catalysts for Carbon Monoxide Oxidation. *Top. Catal.* **2007**, *44*, 167–172. [[CrossRef](#)]
54. Mohite, V.S.; Mahadik, M.A.; Kumbhar, S.S.; Hunge, Y.M.; Kim, J.H.; Moholkar, A.V.; Rajpure, K.Y.; Bhosale, C.H. Photoelectrocatalytic Degradation of Benzoic Acid Using Au Doped TiO₂ Thin Films. *J. Photochem. Photobiol. B Biol.* **2015**, *142*, 204–211. [[CrossRef](#)]
55. Yu, J.C.; Yu, J.; Zhao, J. Enhanced Photocatalytic Activity of Mesoporous and Ordinary TiO₂ Thin Films by Sulfuric Acid Treatment. *Appl. Catal. B Environ.* **2002**, *36*, 31–43. [[CrossRef](#)]
56. Bowers, G.N.; McComb, R.B.; Christensen, R.C.; Schaffer, R. High-Purity 4-Nitrophenol: Purification, Characterization, and Specifications for Use as a Spectrophotometric Reference Material. *Clin. Chem.* **1980**, *26*, 724–729. [[CrossRef](#)]
57. Kumar, A.; Belwal, M.; Maurya, R.R.; Mohan, V.; Vishwanathan, V. Heterogeneous Catalytic Reduction of Anthropogenic Pollutant, 4-Nitrophenol by Au/AC Nanocatalysts. *Mater. Sci. Energy Technol.* **2019**, *2*, 526–531. [[CrossRef](#)]